

Philipp Gaulhofer, BSc

**A preconditioned Schur complement method
for the space-time finite element discretization
of the heat equation**

MASTER'S THESIS

to achieve the university degree of
Diplom-Ingenieur

Master's degree programme:
Mathematics

submitted to
Graz University of Technology

Supervisor

Prof. Dr. O. Steinbach
Institute of Applied Mathematics

Graz, December 2024

AFFIDAVIT

I declare that I have authored this thesis independently, that I have not used other than the declared sources/resources, and that I have explicitly indicated all material which has been quoted either literally or by content from the sources used. The text document uploaded to TUGRAZonline is identical to the present master's thesis.

Date, Signature

Preface

This thesis gave me the chance to deepen my knowledge acquired in my studies of Technomathematics at Graz University of Technology, especially concerning domain decomposition methods for the heat equation in the space-time setting. This work sets out to find a suitable preconditioner for the Schur complement of the heat equation when decomposed into time slabs. Finally, revealing underlying problems with this formulation leads to a modified version that gives us the desired results.

I would like to especially thank Prof. Dr. Olaf Steinbach for already sparking my interest in this topic during work on my Bachelors and continuing to support my endeavors over a long period of time. Additional thanks go to Dipl.-Ing. Michael Reichelt for sharing his codebase with me to build upon and also supporting me with continuous feedback while writing this thesis.

Abstract

This thesis concerns itself with the space-time finite element method for the heat equation. The goal is to find a domain composition approach combined with a suitable preconditioner to develop an efficient parallel solution method. It turns out that using solely algebraic domain decomposition has some problems for the standard finite element formulation of the heat equation. Analysis on the ODE setting provides the idea for a decomposition strictly enforcing time causality. This finally provides promising results.

Diese Arbeit beschäftigt sich mit der Raum-Zeit-Finite-Elemente-Methode für die Wärmeleitgleichung. Das Ziel ist es, einen Gebietszerlegungsansatz in Kombination mit einem geeigneten Vorkonditionierer zu finden, um eine effiziente parallele Lösungsmethode zu entwickeln. Es stellt sich heraus, dass die alleinige Verwendung algebraischer Gebietszerlegung für die Standard-Finite-Elemente-Formulierung der Wärmeleitgleichung einige Probleme mit sich bringt. Eine Analysis auf der ODE-Ebene liefert die Idee für eine Zerlegung, die die Zeitkausalität strikt durchsetzt. Dies liefert schließlich vielversprechende Ergebnisse.

Contents

Introduction	11
1 Preliminaries	13
1.1 Spaces and Norms	13
1.1.1 Bochner Spaces	13
1.1.2 Alternative Norm	14
1.2 Well-Posedness Theorems	15
1.2.1 Lax-Milgram Lemma	15
1.2.2 BBL Condition	16
1.3 Algebraic Domain Decomposition	16
2 A Space-time Finite Element Method for the Heat Equation	19
2.1 Variational Formulation	19
2.1.1 Unique Solvability	20
2.1.2 Discrete Stability	22
2.2 Error Estimate	22
3 ODE Setting	25
3.1 Spatial Eigenvalue Transformation	25
3.2 ODE Setting	26
3.3 Algebraic decomposition	27
3.3.1 Implicit Euler Preconditioner	30
3.3.2 Results	31
3.4 Introducing Strict Time Causality Into The Decomposition	32
3.4.1 Analysis of the Decomposition	33
3.4.2 Results	34
4 PDE Setting	37
4.1 Discretization	37
4.1.1 Baseline Results	39
4.2 Implicit Euler Preconditioner	39
4.3 Results after Preconditioning	41
4.4 Time Causal Space-Time FEM for the Heat Equation	43
4.4.1 Discretization and Matrix Assembly	43
4.4.2 Results	44

5 Conclusion	49
---------------------	-----------

Bibliography	51
---------------------	-----------

Introduction

The primary emphasis of this thesis is on the space-time finite element discretization of the heat equation. Applying conventional finite element methods to time dependent partial differential equations usually means first discretizing the spatial domain and afterwards the temporal domain or conversely first the temporal and then the spatial domain. Space-time finite element methods combine these domains into a generally 4-dimensional problem. Test and ansatz spaces are then defined with no distinction being made between spatial and temporal directions. A lot of work concerning this general setting has been done in [15] [13].

In this work we restrict ourselves to one spatial dimension to end up with a two-dimensional problem. We set a primary goal of implementing domain decomposition methods and preconditioning techniques to develop an efficient parallel solution method. Inspiration for the decomposition into time slices used in this work is taken from the Parareal algorithm first introduced in [9]. Previous work has already shown feasibility of an algebraical domain decomposition for arbitrary domains, see [12].

Chapter 1 introduces necessary function spaces, norms and general results used in space time finite element methods. Also, the algebraic domain composition approach is introduced there. In Chapter 2 we introduce the heat equation, its standard space-time variational formulation and existing stability results following the lines of [11]. Also we give basic error estimates to verify numerical experiments conducted later on. Chapter 3 uses a semi-discretization approach to simplify the model problem to a system of ODEs. This allows us to do more explicit analysis of the domain decomposition, gaining insights into the structure of the Schur complement matrix and revealing some underlying problems with a purely algebraic decomposition. Further, an alternative formulation is introduced to adress these problems. The final Chapter 4 implements a space-time finite element method for the heat equation. There we also apply the insights gained in Chapter 3 to the PDE setting. Finally, we arrive at a appropriately preconditioned formulation for the heat equation.

1 Preliminaries

In this preliminary chapter we introduce the function spaces needed for the space-time finite element method for the heat equation. Further, we discuss different norms on said spaces. We also state standard well-posedness results for both elliptic Galerkin-Bubnov formulations and the Galerkin-Petrov finite element setting. Ending this chapter is a discussion of a basic, purely algebraic domain composition we intend to apply to the discretized heat equation.

1.1 Spaces and Norms

This first Section introduces the spaces and norms needed to provide a variational formulation for the heat equation and the appropriate analysis.

1.1.1 Bochner Spaces

Bochner spaces are an extension of the usual L^p spaces. More on this topic can be found in [6].

Definition 1.1 (Bochner Spaces). Let X be a separable Banach space with norm $\|\cdot\|$. For a bounded subset $D \subset \mathbb{R}^n$ and $p \in [0, \infty)$ define

$$L^p(D, X) = \{f : D \rightarrow X \mid f \text{ is Bochner measurable, } \|f\| \in L^p(D)\}.$$

For time dependent partial differential equations we usually set $D = (0, T)$, $T > 0$.

We now define Sobolev-Bochner spaces using the generalized temporal derivative.

Definition 1.2 (Sobolev-Bochner spaces). For a separable Banach space X with norm $\|\cdot\|$, we define

$$H^1(0, T; X) = \{f \in L^2(0, T; X) \mid \partial_t f \in L^2(0, T; X)\}.$$

We can also introduce initial and terminal conditions to these spaces:

Definition 1.3.

$$\begin{aligned} H_{0,0}^1(0, T; X) &:= \{u \in H^1(0, T; X) \mid u(0) = 0\}, \\ H_{0,T}^1(0, T; X) &:= \{u \in H^1(0, T; X) \mid u(T) = 0\} \end{aligned}$$

Finally we state the spaces later used in the variational formulation for the heat equation and their respective norms.

Let Ω be a bounded Lipschitz domain in \mathbb{R}^d , $d = 1, 2, 3$, we define

$$X = L^2(0, T; H_0^1(\Omega)) \cap H_0^1(0, T; H^{-1}(\Omega)), \quad Y = L^2(0, T; H_0^1(\Omega)),$$

with

$$\begin{aligned} \|v\|_Y^2 &= \|\nabla_x v\|_{L_2(Q)}^2 \\ \|u\|_X^2 &= \|u\|_Y^2 + \|\partial_t u\|_{Y'}^2. \end{aligned}$$

Given these norms the spaces X and Y are Hilbert spaces.

1.1.2 Alternative Norm

Since the norm on X contains the dual norm of Y it is not easily representable. We therefore seek a different representation of the dual norm $\|\cdot\|_{Y'}$.

For $\partial_t u \in Y'$, let $w \in Y$ be the unique solution of the variational formulation to find $w \in Y$ such that

$$\langle \nabla_x w, \nabla_x v \rangle_{L_2(Q)} = \langle \partial_t u, v \rangle_Q \quad \forall v \in Y. \quad (1.1)$$

Unique solvability of this variational formulation can be shown using the Lax Milgram theorem.

Furthermore we can show that $\|w\|_Y \leq \|\partial_t u\|_{Y'}$:

$$\begin{aligned} \|w\|_Y^2 &= \langle \nabla_x w, \nabla_x w \rangle_{L_2(Q)} \\ &= \langle \partial_t u, w \rangle_Q \\ &\leq \|\partial_t u\|_{Y'} \|w\|_Y \\ \Rightarrow \|w\|_Y &\leq \|\partial_t u\|_{Y'}. \end{aligned}$$

Also showing the inequality for the opposite direction $\|\partial_t u\|_{Y'} \leq \|w\|_Y$:

$$\begin{aligned} \|\partial_t u\|_{Y'} &= \sup_{v \in Y, v \neq 0} \frac{\langle \partial_t u, v \rangle_Q}{\|v\|_Y} \\ &= \sup_{v \in Y, v \neq 0} \frac{\langle \nabla_x w, \nabla_x v \rangle_{L_2(Q)}}{\|v\|_Y} \\ &\leq \sup_{v \in Y, v \neq 0} \frac{\|w\|_Y \|v\|_Y}{\|v\|_Y} = \|w\|_Y, \end{aligned}$$

yields $\|\partial_t u\|_{Y'} = \|w\|_Y$.

In a similar way we also define a norm in the discrete setting: For a finite element test

space $Y_h \subset Y$ (e.g. $S_h^1(Q)$), let $w_h \in Y_h$ be the solution of the variational formulation, to find $w_h \in Y_h$ such that

$$\langle \nabla_x w_h, \nabla_x v_h \rangle_{L_2(Q)} = \langle \partial_t u, v_h \rangle_Q \quad \forall v_h \in Y_h. \quad (1.2)$$

The difference between (1.1) and (1.2) gives us the Galerkin orthogonality

$$\langle \nabla_x (w - w_h), \nabla_x v_h \rangle_{L_2(Q)} = 0 \quad \forall v_h \in Y_h.$$

Using this we get:

$$\begin{aligned} 0 &\leq \langle \nabla_x (w - w_h), \nabla_x (w - w_h) \rangle \\ &= \langle \nabla_x (w - w_h), \nabla_x w \rangle \\ &= \langle \nabla_x (w), \nabla_x w \rangle - \langle \nabla_x w_h, \nabla_x w \rangle \\ &= \langle \nabla_x (w), \nabla_x w \rangle - \langle \nabla_x w_h, \nabla_x w_h \rangle \\ &\Rightarrow \|\nabla_x w_h\|_{L^2(Q)}^2 \leq \|\nabla_x w\|_{L^2(Q)}^2, \end{aligned}$$

which finally yields $\|w_h\|_Y \leq \|w\|_Y$. Generally the opposite inequality does not hold true.

Definition 1.4 (Mesh dependent energy norm). For $u \in X$:

$$\|u\|_{X,h}^2 = \|u\|_{L_2(0,T;H_0^1(\Omega))}^2 + \|w_h\|_{L_2(0,T;H_0^1(\Omega))}^2. \quad (1.3)$$

1.2 Well-Posedness Theorems

A standard result concerning well-posedness of a elliptic variational formulation is the Lax-Milgram Lemma:

1.2.1 Lax-Milgram Lemma

For a variational problem with identical test and ansatz space V , i.e. to find $u \in V$ such that

$$a(u, v) = f(v) \quad \forall v \in V, \quad (1.4)$$

well posedness can be shown via the Lax-Milgram Lemma.

Theorem 1.1 (Lax-Milgram Lemma). *Let V be a Hilbert space, $a(\cdot, \cdot) : V \times V \rightarrow \mathbb{R}$ a bounded bilinear form and let $f \in V'$. If the bilinear form a is coercive, i.e.*

$$\exists \alpha > 0, \forall u \in V, a(u, u) \geq \alpha \|u\|_V^2.$$

Then the problem (1.4) is well-posed with the stability estimate for the solution

$$\forall f \in V', \quad \|u\|_V \leq \alpha^{-1} \|f\|_{V'}.$$

Proof. See [3, Lemma 2.2]. □

1.2.2 BBL Condition

Since we are dealing with a variational formulation with different test and ansatz space (Galerkin-Petrov) we need a different way of describing unique solvability than the Lax-Milgram Lemma relying coercivity.

Theorem 1.2 (BBL-condition). *Let U, V be Hilbert spaces, $a : U \times V \rightarrow \mathbb{R}$ a bilinear form and $f \in V'$. Then the variational Problem to find $u \in U$ such that*

$$a(u, v) = \langle f, v \rangle \quad \forall v \in V,$$

is uniquely solvable if and only if:

(i) *The bilinear form $a(\cdot, \cdot)$ is bounded:*

$$\exists c_B > 0 : \quad |a(u, v)| \leq c_B \|u\|_U \|v\|_V \quad \forall u \in U, \forall v \in V. \quad (1.5)$$

(ii) *The bilinear form satisfies the inf-sup condition:*

$$\exists c_S > 0 : \quad \inf_{0 \neq u \in U} \sup_{0 \neq v \in V} \frac{a(u, v)}{\|u\|_U \|v\|_V} \geq c_S. \quad (1.6)$$

(iii) *Surjectivity of the associated operator:*

$$\forall v \in V, v \neq 0 \quad \exists u \in U \quad : \quad a(u, v) \neq 0. \quad (1.7)$$

Proof. See [1, Satz 4.27]. □

Remark 1.1. Condition (1.6) is injectivity of the associated operator, therefore giving us uniqueness of any solution when viewed separately. Further, Condition (1.7) is surjectivity ensuring existence of a solution.

Further (1.2) can be extended to reflexive Banach spaces. see [3, Theorem 2.6].

1.3 Algebraic Domain Decomposition

The starting point for this algebraical decomposition is the linear system of equations resulting from any space-time finite element discretization

$$A \underline{u} = \underline{f}. \quad (1.8)$$

First, we introduce a decomposition of the space time cylinder $Q = \Omega \times (0, T)$ into p non-overlapping subdomains Q_i , $i = 1, \dots, p$ such that:

$$\overline{Q} = \bigcup_{i=1}^p \overline{Q}_i, \quad Q_i \cap Q_j = \emptyset \quad \text{for } i \neq j.$$

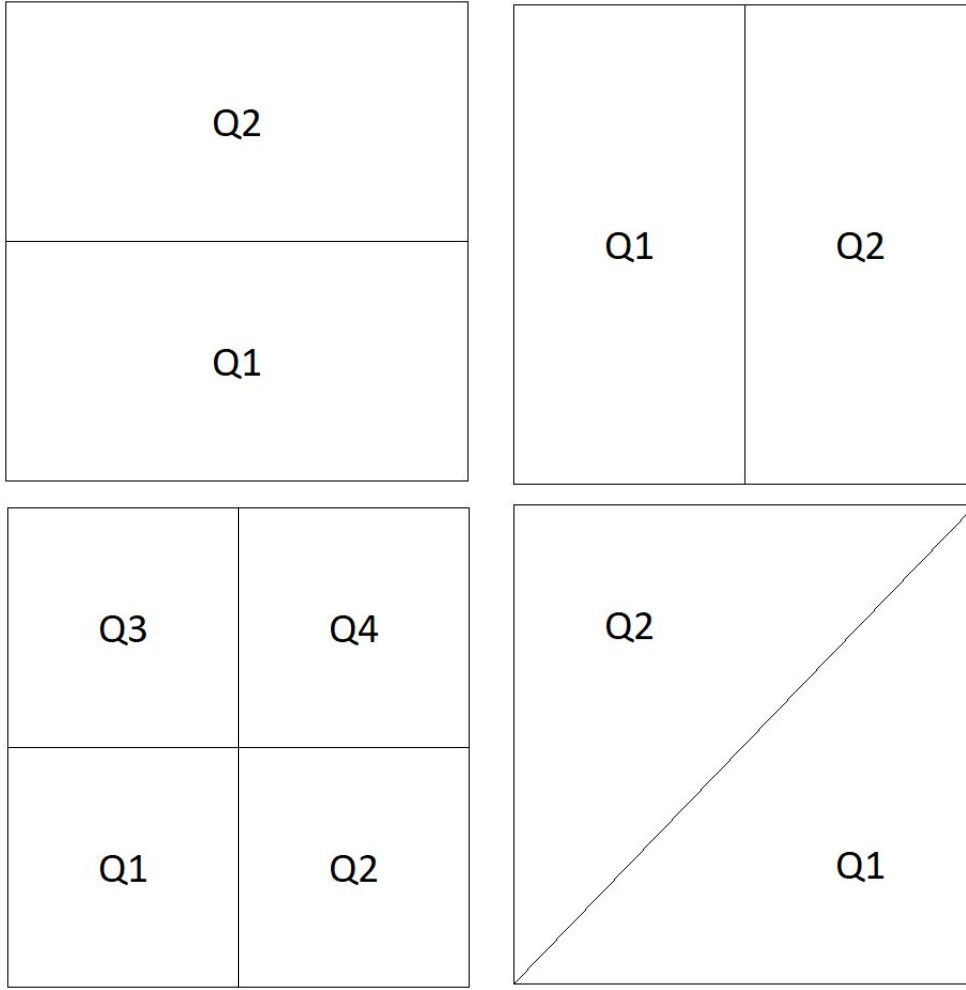


Figure 1.1: Examples of different decompositions of the unit square $(0,1)^2$

For simplicity, this decomposition should be resolved by the finite element mesh, i.e. all boundaries between subdomains $\overline{Q}_i \cap \overline{Q}_j$ should be contained in the edge set of the finite element discretization and corners of the boundaries should be nodes. Examples of such decompositions can be seen in Figure 1.1.

This allows us to reorder the degrees of freedom of both the solution vector \underline{u} and the right hand side \underline{f} into corresponding parts for each subdomain $\underline{u}_{I,i}$, $\underline{f}_{I,i}$ and connecting degrees of freedom \underline{u}_C , \underline{f}_C . Further, we can introduce the collection of all internal dofs:

$$\begin{aligned}\underline{u}_I &= (\underline{u}_{I,1}^\top, \dots, \underline{u}_{I,p}^\top)^\top, \\ \underline{f}_I &= (\underline{f}_{I,1}^\top, \dots, \underline{f}_{I,p}^\top)^\top.\end{aligned}$$

With this simple reordering, we arrive at the block system

$$\begin{pmatrix} A_{II} & A_{CI} \\ A_{IC} & A_{CC} \end{pmatrix} \begin{pmatrix} \underline{u}_I \\ \underline{u}_C \end{pmatrix} = \begin{pmatrix} \underline{f}_I \\ \underline{f}_C \end{pmatrix}. \quad (1.9)$$

Using the fact that we are dealing with a non-overlapping decomposition, we assume that ansatz-/test-functions from different subdomains have non-overlapping supports, which are contained in their respective subdomains. Therefore, A_{II} turns out to be block-diagonal

$$A_{II} = \begin{pmatrix} A_{11} & & & \\ & A_{22} & & \\ & & \ddots & \\ & & & A_{pp} \end{pmatrix}.$$

By eliminating the internal degrees of freedom \underline{u}_I from the block system (1.9), we arrive at the Schur complement system

$$\begin{aligned} S \underline{u}_C &= (A_{CC} - A_{IC} A_{II}^{-1} A_{CI}) \underline{u}_C = \underline{f}_C - A_{IC} A_{II}^{-1} \underline{f}_I = \underline{f}_S, \\ \underline{u}_I &= A_{II}^{-1} \underline{f}_I - A_{II}^{-1} A_{CI} \underline{u}_C. \end{aligned} \quad (1.10)$$

We plan on using an iterative method to solve the system $S \underline{u}_C = \underline{f}_S$.

Multiplying any vector by S involves an application of the inverse of A_{II} . Due to the block diagonal structure, this comes down to solving the local problems A_{11}, \dots, A_{pp} , which can be done completely parallel. Assuming similar sized domains and perfect speedup, we need any iterative method that depends on the application of S to resolve before p iterations, in order to have any kind of advantage over simply solving the local problems in sequence.

2 A Space-time Finite Element Method for the Heat Equation

We consider the heat equation with homogeneous boundary and initial conditions in a bounded Lipschitz domain $\Omega \subset \mathbb{R}^n$ for a finite time interval $(0, T)$, with $T > 0$. Further $Q := \Omega \times (0, T)$ is called the Space-Time Cylinder and $\Sigma := \partial\Omega \times (0, T)$ denotes its lateral boundary. The heat equation then reads as

$$\begin{aligned} \partial_t u(t, x) - \Delta_x u(t, x) &= f(t, x) && \text{for } (t, x) \in Q, \\ u(t, x) &= 0 && \text{for } (t, x) \in \Sigma, \\ u(0, x) &= 0 && \text{for } x \in \Omega. \end{aligned} \quad (2.1)$$

The following section follows the approach presented in [11] with some improvements taken from [7].

2.1 Variational Formulation

In order to obtain a variational formulation we first multiply the heat equation (2.1) by a sufficiently smooth test function and then integrate over the whole space-time cylinder Q to obtain

$$\int_Q \partial_t u(t, x) v(t, x) \, dx dt - \int_Q \Delta_x u(t, x) v(t, x) \, dx dt = \int_Q f(t, x) v(t, x) \, dx dt.$$

Using integration by parts with respect to the spatial variables for the second term yields

$$\begin{aligned} \int_Q \partial_t u(t, x) v(t, x) \, dx dt + \int_Q \nabla_x u(t, x) \cdot \nabla_x v(t, x) \, dx dt \\ - \int_{\Sigma} v(t, x) \nabla_x u(t, x) \cdot n_x \, ds_x dt = \int_Q f(x, t) v(x, t) \, dx dt, \end{aligned}$$

where n_x is the outward pointing unit normal vector on $\partial\Omega$. Setting the test function $v = 0$ on Σ we arrive at

$$\int_Q \partial_t u(t, x) v(t, x) \, dx dt + \int_Q \nabla_x u(t, x) \cdot \nabla_x v(t, x) \, dx dt = \int_Q f(x, t) v(x, t) \, dx dt.$$

The variational formulation of the heat equation then is to find $u \in X$, such that

$$\int_Q \partial_t u(t, x) v(t, x) dx dt + \int_Q \nabla_x u(t, x) \cdot \nabla_x v(t, x) dx dt = \int_Q f(x, t) v(x, t) dx dt, \quad (2.2)$$

$\forall v \in Y.$

The spaces X and Y used here are defined in Section 1.1. For notational brevity, we also define the bilinear form $a(\cdot, \cdot)$ as

$$a(u, v) = \int_Q \partial_t u(t, x) v(t, x) dx dt + \int_Q \nabla_x u(t, x) \cdot \nabla_x v(t, x) dx dt.$$

As X and Y are Gelfand triples with respect to the intermediate Hilbert space $L^2(Q)$ ($Y \subset L^2(Q) \subset Y'$), we can extend the integrals to the duality product $\langle \cdot, \cdot \rangle_Q$ which is well-defined for the chosen spaces [8].

2.1.1 Unique Solvability

To prove unique solvability of the variational formulation (2.2) we intend to verify the BBL-Condition stated in Theorem 1.2. The first condition to check is (1.5) asking for the bilinear form $a(\cdot, \cdot)$ to be bounded, which can be shown by applying Cauchy-Schwarz and Hölder's inequality in the following way:

$$\begin{aligned} a(u, v) &= \langle \partial_t u, v \rangle_Q + \langle \nabla_x u, \nabla_x v \rangle_{L_2(Q)} \\ &\leq \|\partial_t u\|_{Y'} \|v\|_Y + \|u\|_Y \|v\|_Y \\ &= [\|\partial_t u\|_{Y'} + \|u\|_Y] \|v\|_Y \\ &\leq \sqrt{2} [\|\partial_t u\|_{Y'}^2 + \|u\|_Y^2]^{\frac{1}{2}} \|v\|_Y \\ &= \sqrt{2} \|u\|_X \|v\|_Y. \end{aligned}$$

In order to ensure uniqueness of a possible solution we need to fulfil the inf-sup-stability condition (1.6). Consider $u \in X \subset Y$, and let w be the unique solution of the variational formulation (1.1), then

$$\begin{aligned} a(u, u + w) &= \langle \partial_t u, u \rangle_Q + \langle \partial_t u, w \rangle_Q + \langle \nabla_x u, \nabla_x u \rangle_{L_2(Q)} + \langle \nabla_x u, \nabla_x w \rangle_{L_2(Q)} \\ &= \langle \nabla_x w, \nabla_x u \rangle_{L_2(Q)} + \langle \nabla_x w, \nabla_x w \rangle_{L_2(Q)} + \langle \nabla_x u, \nabla_x u \rangle_{L_2(Q)} + \langle \nabla_x u, \nabla_x w \rangle_{L_2(Q)} \\ &= \langle \nabla_x w, \nabla_x (u + w) \rangle_{L_2(Q)} + \langle \nabla_x u, \nabla_x (u + w) \rangle_{L_2(Q)} \\ &= \langle \nabla_x (u + w), \nabla_x (u + w) \rangle_{L_2(Q)} \\ &= \|u + w\|_Y^2. \end{aligned}$$

We can further estimate $\|u + w\|_Y^2$

$$\begin{aligned}\|u + w\|_Y^2 &= \langle \nabla_x u, \nabla_x u \rangle_{L_2(Q)} + \langle \nabla_x w, \nabla_x w \rangle_{L_2(Q)} + 2\langle \nabla_x u, \nabla_x w \rangle_{L_2(Q)} \\ &= \langle \nabla_x u, \nabla_x u \rangle_{L_2(Q)} + \langle \nabla_x w, \nabla_x w \rangle_{L_2(Q)} + 2\langle \partial_t u, u \rangle_Q \\ &\geq \|u\|_Y^2 + \|w\|_Y^2 \\ &= \|u\|_X^2,\end{aligned}$$

since

$$2\langle \partial_t u, u \rangle_Q = \int_0^T \frac{d}{dt} \int_{\Omega} u(x, t)^2 dx dt = \int_{\Omega} u(x, T)^2 dx \geq 0,$$

using $2u\partial_t u = \frac{\partial}{\partial t}[u^2]$ and $u(x, 0) = 0$. For $u \in X$ we therefore get

$$a(u, u + w) \geq \|u + w\|_Y \|u\|_X,$$

which finally yields the desired inf-sup stability condition

$$\begin{aligned}\sup_{0 \neq v \in Y} \frac{a(u, v)}{\|v\|_Y} &\geq \frac{a(u, u + w)}{\|u + w\|_Y} \\ &\geq \frac{\|u\|_X \|u + w\|_Y}{\|u + w\|_Y} \\ &\geq \|u\|_X.\end{aligned}$$

Since this inequality holds for all $u \in X$, this gives us the inf-sup stability constant $c_S = 1$.

In order to fulfill Theorem 1.2, it still remains to show (1.7). For this purpose, let $0 \neq v \in Y$ and define $\bar{u}(x, t) = \int_0^t v(x, s) ds$. One can easily see that $\partial_t \bar{u} = v$ and therefore $\bar{u} \in X$. Now,

$$\begin{aligned}a(\bar{u}, v) &= \langle \partial_t \bar{u}, v \rangle_Q + \int_0^T \int_{\Omega} \nabla_x \bar{u} \cdot \nabla_x v dx dt \\ &= \langle v, v \rangle_Q + \int_0^T \int_{\Omega} \nabla_x \bar{u} \cdot \nabla_x \partial_t \bar{u} dx dt \\ &= \|v\|_{L^2(Q)}^2 + \int_0^T \frac{1}{2} \frac{d}{dt} \int_{\Omega} |\nabla_x \bar{u}|^2 dx dt \\ &= \|v\|_{L^2(Q)}^2 + \frac{1}{2} \int_{\Omega} |\nabla_x \bar{u}(\cdot, T)|^2 dx \\ &\geq \|v\|_{L^2(Q)}^2 + \frac{1}{2} \|\nabla_x \bar{u}(\cdot, T)\|_{L^2(\Omega)}^2 > 0,\end{aligned}$$

which implies the desired surjectivity condition (1.7) and concludes the proof.

2.1.2 Discrete Stability

For the discretization of (2.2) we use conforming test and ansatz spaces $X_h \subset X$, $Y_h \subset Y$. We also assume $X_h \subset Y_h$ and $\dim(X_h) = \dim(Y_h) < \infty$ to end up with the variational problem, to find $u_h \in X_h$, such that

$$\langle \partial_t u_h, v_h \rangle_Q + \langle \nabla_x u_h, \nabla_x v_h \rangle_{L_2(Q)} = \langle f, v_h \rangle_Q \quad \forall v_h \in Y_h. \quad (2.3)$$

Using the mesh dependent energy norm (1.3) we are able to prove a discrete inf-sup condition following similar steps as in the continuous case. For $u_h \in X_h \subset X$ we have $w_h \in Y_h$ from (1.2). With $X_h \subset Y_h$ we get $(u_h + w_h) \in Y_h$ and hence

$$\begin{aligned} a(u_h, u_h + w_h) &= \langle \nabla_x w_h, \nabla_x u_h \rangle_{L_2(Q)} + \langle \nabla_x w_h, \nabla_x w_h \rangle_{L_2(Q)} \\ &\quad + \langle \nabla_x u_h, \nabla_x u_h \rangle_{L_2(Q)} + \langle \nabla_x u_h, \nabla_x w_h \rangle_{L_2(Q)} \\ &= \langle \nabla_x (u_h + w_h), \nabla_x (u_h + w_h) \rangle_{L_2(Q)} \\ &= \|u_h + w_h\|_Y^2. \end{aligned}$$

Again estimating $\|u + w\|_Y^2$ from below yields

$$\begin{aligned} \|u_h + w_h\|_Y^2 &= \langle \nabla_x u_h, \nabla_x u_h \rangle_{L_2(Q)} + \langle \nabla_x w_h, \nabla_x w_h \rangle_{L_2(Q)} + 2\langle \partial_t u_h, u_h \rangle_Q \\ &\geq \|u_h\|_Y^2 + \|w_h\|_Y^2 \\ &= \|u_h\|_{X,h}^2. \end{aligned}$$

We therefore get

$$a(u_h, u_h + w_h) \geq \|u_h + w_h\|_Y \|u_h\|_{X,h},$$

resulting in the discrete inf-sup stability condition

$$\sup_{0 \neq v_h \in Y_h} \frac{a(u_h, v_h)}{\|v_h\|_Y} \geq \frac{a(u_h, u_h + w_h)}{\|u_h + w_h\|_Y} \geq \|u_h\|_{X,h}. \quad (2.4)$$

This also yields the discrete inf-sup stability constant $c_S = 1$

Since we requested X_h and Y_h to be of the same dimension, the equivalent system of linear equations is square. The standard choice $X_h = Y_h$ also trivially fulfils this condition. Finally, using (2.4) we can deduce injectivity and therefore unique solvability of the discrete system (2.3).

2.2 Error Estimate

Combining the variational formulations (2.2) and (2.3) using $Y_h \subset Y$ we can conclude Galerkin orthogonality

$$a(u - u_h, v_h) = 0 \quad \forall v_h \in Y_h.$$

Theorem 2.1 (Cea's Lemma). *Let $\bar{u} \in X$ and $\bar{u}_h \in X_h$ be the unique solutions to the variational problems (2.2) and (2.3) respectively, then there holds the quasi optimal error-estimate:*

$$\|\bar{u} - \bar{u}_h\|_{X,h} \leq (1 + \sqrt{2}) \inf_{z_h \in X_h} \|\bar{u} - z_h\|_X. \quad (2.5)$$

Proof. Let $z_h \in X_h$, we have

$$\begin{aligned} \|\bar{u} - \bar{u}_h\|_{X,h} &\leq \|\bar{u} - z_h\|_{X,h} + \|z_h - \bar{u}_h\|_{X,h} \\ &\leq \|\bar{u} - z_h\|_X + \|z_h - \bar{u}_h\|_{X,h}. \end{aligned}$$

Using the discrete inf-sup stability condition in the second term further yields

$$\begin{aligned} \|z_h - \bar{u}_h\|_{X,h} &\leq \sup_{0 \neq v \in Y_h} \frac{a(z_h - \bar{u}_h, v_h)}{\|v_h\|_Y} \\ &= \sup_{0 \neq v \in Y_h} \frac{a(z_h - \bar{u}, v_h)}{\|v_h\|_Y} \\ &\leq \sup_{0 \neq v \in Y_h} \frac{\sqrt{2} \|z_h - \bar{u}\|_X \|v_h\|_Y}{\|v_h\|_Y} \\ &= \sqrt{2} \|z_h - \bar{u}\|_X \end{aligned}$$

where we used Galerkin orthogonality in the second and boundedness of $a(\cdot, \cdot)$ in the third step.

Combining the terms again concludes the proof:

$$\begin{aligned} \|\bar{u} - \bar{u}_h\|_{X,h} &\leq \|\bar{u} - z_h\|_X + \|z_h - \bar{u}_h\|_{X,h} \\ &\leq (1 + \sqrt{2}) \|\bar{u} - z_h\|_X \end{aligned}$$

□

For simplicity we consider the space-time cylinder $Q = \Omega \times (0, T) \subset \mathbb{R}^{n+1}$ to have a polygonal/polyhedral boundary depending on n . We introduce a decomposition Q_h of Q into simplicial finite elements q_l . By $\Delta_l := \int_{q_l} dx dt$ we denote the volume of the finite element q_l and the local and global mesh width as $h_l := \Delta_l^{1/(n+1)}$ and $h := \max_{l=1, \dots, N} h_l$ respectively. Finally we can introduce the space-time finite element space $S_h^1(Q_h)$ of piecewise linear, globally continuous basis functions ψ_k . Using Cea's Lemma and basic approximation properties we can then obtain the following energy error estimate

Theorem 2.2 (Energy error estimate). *Let $\bar{u} \in X$ and $\bar{u}_h \in X_h = S_h^1(Q_h) \cap X$ be the unique solutions to the variational problems (2.2) and (2.3) respectively. Further, let $\bar{u} \in H^2(Q)$, then there holds the error-estimate in the energy norm:*

$$\|\bar{u} - \bar{u}_h\|_Y = \|\nabla_x(\bar{u} - \bar{u}_h)\|_{L_2(Q)} \leq ch |\bar{u}|_{H^2(Q)}. \quad (2.6)$$

Proof. See [11, Thm 3.3].

□

3 ODE Setting

In the previous Chapter, we have introduced a space-time finite element method for the heat equation. In order to gain a deeper insight into the structure of the resulting matrices and also the domain decomposition introduced in Section 1.3, it is helpful to transition to the ODE setting. For this, we apply a semi discretization approach.

3.1 Spatial Eigenvalue Transformation

To transform the heat equation (2.1) from a PDE to a system of ODEs, we follow a similar approach as in [14, Section 3], by using the eigenfunctions of the Laplacian $\psi_i \in H_0^1(\Omega)$

$$\begin{aligned} -\Delta_x \psi_i(x) &= \mu_k \psi_i(x), & x \in \Omega, \\ \psi_i(x) &= 0, & x \in \partial\Omega. \\ \|\psi_i\|_{L^2(\Omega)} &= 1 \end{aligned}$$

We should note that the eigenfunctions ψ_i form an orthonormal basis in $L_2(\Omega)$ and a orthogonal basis in $H_0^1(\Omega)$. Without loss of generality we can sort the eigenvalues in ascending order

$$0 < \mu_1 \leq \mu_2 \leq \dots$$

Using the ansatz

$$u(t, x) = \sum_{i=1}^{\infty} U_i(t) \psi_i(x), \quad U_i(t) = \int_{\Omega} u(t, x) \psi_i(x) dx,$$

in the variational formulation (2.2) and applying the test function $v(t, x) = V_j(t)\psi_j(x)$, we get:

$$\begin{aligned}
a(u, V_j\psi_j) &= \sum_{i=1}^{\infty} a(U_i\psi_i, V_j\psi_j) \\
&= \sum_{i=1}^{\infty} \int_Q \partial_t(U_i(t)\psi_i(x))V_j(t)\psi_j(x)dxdt + \int_Q \nabla_x(U_i(t)\psi_i(x)) \cdot \nabla_x(V_j(t)\psi_j(x))dxdt \\
&= \sum_{i=1}^{\infty} \int_0^T \partial_t U_i(t)V_j(t)dt \int_{\Omega} \psi_i(x)\psi_j(x)dx + \int_0^T U_i(t)V_j(t)dt \int_{\Omega} \nabla_x\psi_i(x) \cdot \nabla_x\psi_j(x)dx \\
&= \int_0^T [\partial_t U_j(t) + \mu_j U_j(t)]V_j(t)dt = \int_0^T \int_{\Omega} f(x, t)\psi_j(x)dxV_j(t)dt \\
&=: \int_0^T F_j(t)V_j(t)dt.
\end{aligned}$$

As V_j is arbitrary, this is a weak formulation of the ODE

$$\begin{aligned}
\partial_t U_i(t) + \mu_i U_i(t) &= F_i(t), & t \in (0, T), \\
U(0) &= 0,
\end{aligned}$$

which we have to solve for every eigenvalue $\mu_i > 0$.

3.2 ODE Setting

Based on the results above and setting the final time $T = 1$, the following ODE proves to be of interest

$$\begin{aligned}
\partial_t u(t) + \mu u(t) &= f(t), & t \in (0, 1), \\
u(0) &= 0, \\
\mu &> 0.
\end{aligned} \tag{3.1}$$

We derive a weak formulation from this by multiplying with a test function and integrating over $(0, T)$, resulting in the variational problem to find $u \in X$, such that

$$\int_0^1 \partial_t u(t)v(t)dt + \mu \int_0^1 u(t)v(t)dt = \int_0^1 f(t)v(t)dt \quad \forall v \in Y, \tag{3.2}$$

with $X = H_0^1(0, 1) = \{v \in H^1(0, 1) : v(0) = 0\}$ and $Y = L^2(0, 1)$.

For the discretization we use a uniform decomposition $\mathcal{T}_h = \{\tau_k\}_{k=1}^{n_t}$ of $(0, 1)$ into n_t intervals τ_k of length $h = 1/n_t$. A common stable discretization is to discretize X with piecewise linear and continuous functions and Y with piecewise constant functions.

However, this does not resemble the discretization on the PDE level, which corresponds to piecewise linear continuous functions for both X and Y . As in the PDE case $X_h \subset X \subset Y$, so we may investigate the variational problem to find $u_h \in X_h = S_h^1(0, 1) \cap H_{0,1}^1(0, 1)$, such that

$$\int_0^1 \partial_t u_h(t) v_h(t) dt + \mu \int_0^1 u_h(t) v_h(t) dt = \int_0^1 f(t) v_h(t) dt \quad \forall v_h \in X_h.$$

At last, we obtain the linear system of equations

$$(A_h + \mu M_h) \underline{u} = \underline{f}, \quad (3.3)$$

where

$$A_h = \frac{1}{2} \begin{pmatrix} 0 & -1 & & \\ 1 & \ddots & \ddots & \\ & \ddots & 0 & -1 \\ & & 1 & 1 \end{pmatrix}, \quad M_h = \frac{h}{6} \begin{pmatrix} 4 & 1 & & \\ 1 & \ddots & \ddots & \\ & \ddots & 4 & 1 \\ & & 1 & 2 \end{pmatrix}.$$

3.3 Algebraic decomposition

We now apply the decomposition approach presented in Chapter 1.3 to the system (3.3). For simplicity, we split the interval $(0, 1)$ into only $p = 2$ subdomains, but all computations carry over to the general case with arbitrary p .

First, we reorder the dofs into interior ones \underline{u}_I and the ones belonging to the interface \underline{u}_C using a permutation matrix P , such that

$$\begin{pmatrix} \underline{u}_I \\ \underline{u}_C \end{pmatrix} = P \underline{u}.$$

We use this to restructure the system of linear equations

$$A \underline{u} = \underline{f} \iff AP^{-1} \begin{pmatrix} \underline{u}_I \\ \underline{u}_C \end{pmatrix} = \underline{f} \iff \begin{pmatrix} A_{11} & A_{12} \\ A_{21} & A_{22} \end{pmatrix} \begin{pmatrix} \underline{u}_I \\ \underline{u}_C \end{pmatrix} = \begin{pmatrix} \underline{f}_I \\ \underline{f}_C \end{pmatrix}.$$

The Schur complement S can be extracted from this system by eliminating the interior degrees of freedom \underline{u}_I , yielding

$$S \underline{u}_C = (A_{22} - A_{12} A_{11}^{-1} A_{21}) \underline{u}_C = \underline{f}_C - A_{12} A_{11}^{-1} \underline{f}_I = \underline{f}_S. \quad (3.4)$$

We now introduce a notation for different parts of the system matrix A , which can be viewed as being block-tridiagonal

$$A \underline{u} = \begin{pmatrix} A_D & C_{DI} & & \\ B_{DI} & \gamma^1 & C_{ID} & \\ & B_{ID} & A_D & C_{DI} \\ & & B_{DI} & \gamma^2 \end{pmatrix} \begin{pmatrix} \underline{u}_I^1 \\ \underline{u}_C^1 \\ \underline{u}_I^2 \\ \underline{u}_C^2 \end{pmatrix} = \begin{pmatrix} \underline{f}_I^1 \\ \underline{f}_C^1 \\ \underline{f}_I^2 \\ \underline{f}_C^2 \end{pmatrix} \quad (3.5)$$

with

$$A_D = \frac{1}{2} \begin{pmatrix} 0 & -1 & & \\ 1 & \ddots & \ddots & \\ & \ddots & \ddots & -1 \\ & & 1 & 0 \end{pmatrix} + \frac{\mu h}{6} \begin{pmatrix} 4 & 1 & & \\ 1 & \ddots & \ddots & \\ & \ddots & \ddots & 1 \\ & & 1 & 4 \end{pmatrix}$$

$$\begin{aligned} \gamma^1 &= 4\frac{\mu h}{6} = 2\frac{\mu h}{3} & \gamma^2 &= \gamma^1 + \frac{1}{2} = \frac{4\mu h + 3}{6} \\ \kappa_l &= \left(\frac{\mu h}{6} + \frac{1}{2}\right) & \kappa_r &= \left(\frac{\mu h}{6} - \frac{1}{2}\right) \\ B_{DI} &= \kappa_l \underline{e}_{n_s}^T & B_{ID} &= \kappa_l \underline{e}_1 \\ C_{DI} &= \kappa_r \underline{e}_{n_s} & C_{ID} &= \kappa_r \underline{e}_1^T, \end{aligned}$$

where u_C^1 denotes the node at the interface between the first and second subdomain, and u_C^2 the final node at $t = 1$. Using this notation, we can represent the internal degrees of freedom \underline{u}_I^1 and \underline{u}_I^2 from (3.5) explicitly

$$\begin{aligned} \underline{u}_I^1 &= A_D^{-1} \underline{f}_I^1 - A_D^{-1} C_{DI} u_I^1, \\ \underline{u}_I^2 &= A_D^{-1} \underline{f}_I^2 - A_D^{-1} C_{DI} u_I^2 - A_D^{-1} B_{ID} u_I^1. \end{aligned}$$

Inserting this into the equations for the interface node u_C^1 yields

$$\begin{aligned} f_C^1 &= B_{DI} \underline{u}_I^1 + \gamma^1 u_C^1 + C_{ID} \underline{u}_I^2 \\ &= B_{DI} (A_D^{-1} \underline{f}_I^1 - A_D^{-1} C_{DI} u_C^1) + \gamma^1 u_C^1 + C_{ID} (A_D^{-1} \underline{f}_I^2 - A_D^{-1} C_{DI} u_C^2 - A_D^{-1} B_{ID} u_C^1) \\ &\iff \\ \tilde{f}_I^1 &:= f_C^1 - B_{DI} A_D^{-1} \underline{f}_I^1 - C_{ID} A_D^{-1} \underline{f}_I^2 = \\ &= (\gamma^1 - B_{DI} A_D^{-1} C_{DI} - C_{ID} A_D^{-1} B_{ID}) u_C^1 - (C_{ID} A_D^{-1} C_{DI}) u_C^2, \end{aligned}$$

and using the result of some side computations listed below

$$\begin{aligned} B_{DI} A_D^{-1} C_{DI} &= \kappa_l \underline{e}_{n_s}^T A_D^{-1} \kappa_r \underline{e}_{n_s} \\ &= \kappa_l \kappa_r A_D^{-1} [n_s, n_s], \\ C_{ID} A_D^{-1} B_{ID} &= \kappa_l \kappa_r A_D^{-1} [1, 1], \\ C_{ID} A_D^{-1} C_{DI} &= \kappa_r^2 A_D^{-1} [1, n_s], \end{aligned}$$

we arrive at one of the interface equations

$$\tilde{f}_I^1 = (\gamma^1 - \kappa_l \kappa_r (A_D^{-1} [n_s, n_s] + A_D^{-1} [1, 1])) u_C^1 - \kappa_r^2 A_D^{-1} [1, n_s] u_C^2.$$

Following the same approach, we can apply this to the general setting with $p > 2$. When decomposing the computational domain into p subdomains, we obtain the following representation for the internal degrees of freedom

$$\begin{aligned}\underline{u}_I^k &= A_D^{-1}(\underline{f}_I^k - B_{ID}u_C^{k-1} - C_{DI}u_C^k) \\ &= A_D^{-1}(\underline{f}_I^k - \kappa_l \underline{e}_1 u_C^{k-1} - \kappa_r \underline{e}_{n_s} u_C^k).\end{aligned}\tag{3.6}$$

Again, we can insert this into one of the inner interface equations

$$\begin{aligned}f_C^k &= B_{DI}\underline{u}_I^k + \gamma^1 u_C^k + C_{ID}\underline{u}_I^{k+1} = \kappa_l \underline{e}_{n_s}^\top \underline{u}_I^k + \gamma^1 u_C^k + \kappa_r \underline{e}_1^\top \underline{u}_I^{k+1} \\ &= \kappa_l \underline{e}_{n_s}^\top A_D^{-1}(\underline{f}_I^k - \kappa_l \underline{e}_1 u_C^{k-1} - \kappa_r \underline{e}_{n_s} u_C^k) + \gamma^1 u_C^k \\ &\quad + \kappa_r \underline{e}_1^\top A_D^{-1}(\underline{f}_I^{k+1} - \kappa_l \underline{e}_1 u_C^k - \kappa_r \underline{e}_{n_s} u_C^{k+1}),\end{aligned}$$

which we rearrange

$$\begin{aligned}\tilde{f}_C^k &= (-\kappa_l \underline{e}_{n_s}^\top A_D^{-1} \kappa_l \underline{e}_1 u_C^{k-1} - \kappa_l \underline{e}_{n_s}^\top A_D^{-1} \kappa_r \underline{e}_{n_s} u_C^k) + \gamma^1 u_C^k \\ &\quad + (-\kappa_r \underline{e}_1^\top A_D^{-1} \kappa_l \underline{e}_1 u_C^k - \kappa_r \underline{e}_1^\top A_D^{-1} \kappa_r \underline{e}_{n_s} u_C^{k+1}) \\ &= -\kappa_l \underline{e}_{n_s}^\top A_D^{-1} \kappa_l \underline{e}_1 u_C^{k-1} + (\gamma^1 - \kappa_l \underline{e}_{n_s}^\top A_D^{-1} \kappa_r \underline{e}_{n_s} - \kappa_r \underline{e}_1^\top A_D^{-1} \kappa_l \underline{e}_1) u_C^k \\ &\quad - \kappa_r \underline{e}_1^\top A_D^{-1} \kappa_r \underline{e}_{n_s} u_C^{k+1},\end{aligned}$$

to finally derive the general interface equation:

$$\begin{aligned}\tilde{f}_C^k &= \{\gamma^k - \kappa_l \kappa_r (A_D^{-1}[1, 1] + A_D^{-1}[n, n])\} u_C^k \\ &\quad - (\kappa_r^2 A_D^{-1}[1, n]) u_C^{k+1} - (\kappa_l^2 A_D^{-1}[n, 1]) u_C^{k-1}\end{aligned}\tag{3.7}$$

with

$$\begin{aligned}\gamma^k &= \frac{4\mu h}{6}, \quad k \leq p-1 \\ \gamma^p &= \frac{4\mu h + 3}{6}.\end{aligned}$$

This analysis reveals, that the matrix S maintains the tri-diagonal structure of the system matrix A . Moreover, only a few specific entries from the inverse local matrix A_D^{-1} , along with the eigenvalue μ and the grid size h are reflected in its entries.

Using (3.6), we can compute the internal degrees of freedom from their respective interface values via

$$\underline{u}_I^k = A_D^{-1} \underline{f}_I^k - A_D^{-1}(\kappa_l \underline{e}_1 u_C^{k-1} + \kappa_r \underline{e}_{n_s} u_C^k).$$

Since A_D represents a homogenized system matrix for the ODE (3.1), we can interpret $A_D^{-1}(\kappa_l \underline{e}_1 u_C^{k-1} + \kappa_r \underline{e}_{n_s} u_C^k)$ as a discrete solution of:

$$\begin{aligned}\partial_t u(t) + \mu u(t) &= 0 \quad t \in (t_{k-1}, t_k), \\ u(t_{k-1}) &= \kappa_l u_C^{k-1}, \\ u(t_k) &= \kappa_r u_C^k.\end{aligned}$$

Obviously the boundary value problem above is over-constrained, as one can easily see from looking at the general homogeneous solution to the ODE: $u(t) = ce^{-\mu t}$. Generally, this cannot satisfy both boundary conditions simultaneously. This means that, in order for a solution to exist the boundary conditions themselves have to line up in a specific manner.

3.3.1 Implicit Euler Preconditioner

Since the domain decomposition introduces a coarse time step $H = 1/p$, using a time propagation scheme as preconditioner seems to be a good idea. A simple choice is the implicit Euler scheme:

For the ODE $\partial_t w(t) = g(t, w(t))$, $w(0) = 0$, and step size H it reads as

$$\begin{aligned} w_H(0) &= 0 \\ w_H(t_{k+1}) &= w_H(t_k) + Hg(t_{k+1}, w_H(t_{k+1})) \end{aligned}$$

with $t_k = kH$.

After rearranging ODE (3.1) to the form

$$\partial_t u(t) = f(t) - \mu u(t),$$

we can apply the implicit Euler scheme to obtain

$$\begin{aligned} u^0 &= 0 \\ u^{k+1} &= u^k + H[f(t_{k+1}) - \mu u^{k+1}], \end{aligned} \tag{3.8}$$

with $u^k = u_H(t_k)$.

Instead of solving (3.8) recursively, we can reformulate the implicit Euler scheme as a system of linear equations

$$P_I \underline{u} = \underline{f},$$

where

$$P_I = \frac{1}{H} \begin{pmatrix} (1 + H\mu) & & & \\ -1 & (1 + H\mu) & & \\ & \ddots & \ddots & \\ & & -1 & (1 + H\mu) \end{pmatrix}, \quad \underline{u} = \begin{pmatrix} u^1 \\ u^2 \\ \vdots \\ u^{nt} \end{pmatrix}, \quad \underline{f} = \begin{pmatrix} f^1 \\ f^2 \\ \vdots \\ f^{nt} \end{pmatrix}.$$

We will use the system matrix as a left preconditioner for the Schur complement system (3.4), i.e. we will need to analyze the properties of

$$P_I^{-1} S u_C = P_I^{-1} f_S.$$

3.3.2 Results

The method described above has been implemented in Octave [2].

Table 3.1 shows the resulting spectral condition number with respect to different Eigenvalues μ and $p \in \{4, 8\}$. As expected, small μ results in the worst conditioning, with larger eigenvalues yielding a well-conditioned Schur complement S , even without the preconditioner P . We observe, that the number of local degrees of freedom in each subdomain plays an important role. In case of an uneven number of local degrees of freedom, we observe good conditioning in general, and additionally a beneficial effect of the preconditioner. For an even number of local degrees of freedom on the other hand, we can see that the Schur complement itself is already better conditioned and the application of the implicit Euler preconditioner actually degrades the spectral condition number.

4 domains	$n_t = 8$	uneven	4 domains	$n_t = 12$	even
μ	$\kappa_2(S_C)$	$\kappa_2(P_I^{-1}S_C)$	μ	$\kappa_2(S_C)$	$\kappa_2(P_I^{-1}S_C)$
4	4.63668	2.66903	4	1.83566	3.5089
6	3.27453	2.03163	6	1.77831	3.09198
9	2.34836	1.58841	9	1.72092	2.6498
13.5	1.79548	1.3245	13.5	1.57558	2.17411
20.25	1.49881	1.19548	20.25	1.38981	1.75422
8 domains	$n_t = 16$	uneven	8 domains	$n_t = 24$	even
μ	$\kappa_2(S_C)$	$\kappa_2(P_I^{-1}S_C)$	μ	$\kappa_2(S_C)$	$\kappa_2(P_I^{-1}S_C)$
4	20.0658	6.79749	4	3.45582	7.60386
6	12.5822	4.71183	6	2.89656	6.49959
9	7.50748	3.2449	9	2.4724	5.49855
13.5	4.46981	2.27134	13.5	2.22492	4.48512
20.25	2.83164	1.6829	20.25	2.04277	3.47056

Table 3.1: Comparison of spectral condition number for the Schur complement S , with and without left preconditioner P . Insight into an even/uneven number of local degrees of freedom.

Since the influence of the local system matrices on the Schur complement is limited (as seen in (3.7)), we can have a look at the few matrix entries involved in the interface equation. In Table 3.2, we can see how the top right entry of the matrix switches signs when using either an even or uneven number of local degrees of freedom. In contrast, the bottom left entry stays positive for both cases. Indeed, when inspecting the whole matrix, we can identify a checker-board pattern in the upper right triangle, reminiscent of commonly known checker-board instabilities (See e.g. [3, Section 4.2.3]).

4 domains	$n_t = 8$	uneven	4 domains	$n_t = 12$	even
μ	$A[n, 1]$	$A[1, n]$	μ	$A^{-1}[n, 1]$	$A^{-1}[1, n]$
4	3	3	4	1.5	-1.875
6	2	2	6	1.17647	-1.64706
9	1.33333	1.33333	9	0.774194	-1.29032
13.5	0.888889	0.888889	13.5	0.40201	-0.884422
20.25	0.592593	0.592593	20.25	0.152277	-0.543848
8 domains	$n_t = 16$	uneven	8 domains	$n_t = 24$	even
μ	$A^{-1}[n, 1]$	$A^{-1}[1, n]$	μ	$A^{-1}[n, 1]$	$A^{-1}[1, n]$
4	6	6	4	1.80531	-2.0177
6	4	4	6	1.66038	-1.96226
9	2.66667	2.66667	9	1.41772	-1.82278
13.5	1.77778	1.77778	13.5	1.06394	-1.55499
20.25	1.18519	1.18519	20.25	0.657436	-1.17195

Table 3.2: Entries of the inverse system matrix for even/uneven number of local degrees of freedom and different number of decompositions

3.4 Introducing Strict Time Causality Into The Decomposition

Addressing the behaviour observed for the purely algebraic decomposition, e.g over-constrained local problems after the decomposition and odd/even stability issues, we introduce a different approach. To attain this goal, we introduce a domain decomposition at the level of the continuous formulation. The coupling is established through the initial condition, keeping strict time causality, which we believe will enhance stability. This strategy may also mitigate the odd/even problems, suspected in the previous section.

For a time decomposition of the interval $(0, 1)$ into p time slabs: $0 = T_0 < T_1 < \dots < T_p = 1$, we formulate each local problem:

$$\begin{aligned}
 \partial_t u_m(t) + \mu u_m(t) &= f(t) & t \in (T_{m-1}, T_m) \\
 u_m(T_{m-1}) &= u_{m-1}(T_{m-1}) \\
 u_0(0) &= 0,
 \end{aligned}$$

for $m = 1, \dots, p$.

We are now looking at an explicit initial value problem on each subdomain. This avoids the pitfalls of purely algebraic domain decomposition, where the local problems take the form of a boundary value problem and therefore seem over-constrained.

The local matrices are of the same form as the global system:

$$(A_h^m + \mu M_h^m) \underline{u}^m =: H_h^m \underline{u}^m = \underline{f}^m,$$

with

$$A_h^m = \frac{1}{2} \begin{pmatrix} 0 & -1 & & \\ 1 & \ddots & \ddots & \\ & \ddots & 0 & -1 \\ & & 1 & 1 \end{pmatrix}, \quad M_h^m = \frac{h}{6} \begin{pmatrix} 4 & 1 & & \\ 1 & \ddots & \ddots & \\ & \ddots & 4 & 1 \\ & & 1 & 2 \end{pmatrix}.$$

Combining the local matrices with their coupling terms results in the global system matrix

$$H_h = \begin{pmatrix} H_h^1 & & & \\ c & H_h^2 & & \\ & \ddots & \ddots & \\ & & c & H_h^p \end{pmatrix}$$

with $c = (-\frac{1}{2} + \mu \frac{h}{6}) \underline{e}_1^T \underline{e}_{n_s}$.

In contrast to the purely algebraic decomposition, we have no coupling terms above the diagonal, meaning that matrix has a causal structure.

3.4.1 Analysis of the Decomposition

We again calculate the interface equations explicitly using the notation already introduced in (3.5) yielding

$$H_h \underline{u} = \begin{pmatrix} A_D & C_{DI} & & \\ B_{DI} & \gamma^1 & C_{ID} & \\ & B_{ID} & A_D & C_{DI} \\ & & B_{DI} & \gamma^2 \end{pmatrix} \begin{pmatrix} \underline{u}_I^1 \\ \underline{u}_C^1 \\ \underline{u}_I^2 \\ \underline{u}_C^2 \end{pmatrix} = \begin{pmatrix} \underline{f}_I^1 \\ \underline{f}_C^1 \\ \underline{f}_I^2 \\ \underline{f}_C^2 \end{pmatrix} \quad (3.9)$$

with

$$A_D = \frac{1}{2} \begin{pmatrix} 0 & -1 & & \\ 1 & \ddots & \ddots & \\ & \ddots & \ddots & -1 \\ & & 1 & 0 \end{pmatrix} + \frac{\mu h}{6} \begin{pmatrix} 4 & 1 & & \\ 1 & \ddots & \ddots & \\ & \ddots & \ddots & 1 \\ & & 1 & 4 \end{pmatrix}$$

$$\begin{aligned}
\gamma^1 &= \gamma^2 = \frac{1}{2} + 2\frac{\mu h}{6} \\
\kappa_l &= \left(\frac{\mu h}{6} + \frac{1}{2}\right) & \kappa_r &= \left(\frac{\mu h}{6} - \frac{1}{2}\right) \\
B_{DI} &= \kappa_l \underline{e}_{n_s}^T & B_{ID} &= \kappa_l \underline{e}_1 \\
C_{DI} &= \kappa_r \underline{e}_{n_s} & C_{ID} &= 0 \underline{e}_1^T.
\end{aligned}$$

Skipping directly to the general representation of the internal degrees of freedom (3.6), which stay unchanged

$$\underline{u}_I^k = A_D^{-1}(\underline{f}_I^k - \kappa_l \underline{e}_1 u_C^{k-1} - \kappa_r \underline{e}_{n_s} u_C^k),$$

inserting it into the general interface equation

$$\begin{aligned}
f_C^k &= B_{DI} \underline{u}_I^k + \gamma^1 u_C^k = \kappa_l \underline{e}_{n_s}^\top \underline{u}_I^k + \gamma^1 u_C^k \\
&= \kappa_l \underline{e}_{n_s}^\top A_D^{-1}(\underline{f}_I^k - \kappa_l \underline{e}_1 u_C^{k-1} - \kappa_r \underline{e}_{n_s} u_C^k) + \gamma^1 u_C^k
\end{aligned}$$

and further rearranging

$$\begin{aligned}
\tilde{f}_C^k &= (-\kappa_l \underline{e}_{n_s}^\top A_D^{-1} \kappa_l \underline{e}_1 u_C^{k-1} - \kappa_l \underline{e}_{n_s}^\top A_D^{-1} \kappa_r \underline{e}_{n_s} u_C^k) + \gamma^1 u_C^k \\
&= -\kappa_l \underline{e}_{n_s}^\top A_D^{-1} \kappa_l \underline{e}_1 u_C^{k-1} + (\gamma^1 - \kappa_l \underline{e}_{n_s}^\top A_D^{-1} \kappa_r \underline{e}_{n_s}) u_C^k
\end{aligned}$$

uncovers the general interface equation

$$-\kappa_l^2 A_D^{-1}[n, 1] u_C^{k-1} + (\gamma^k - \kappa_l \kappa_r + A_D^{-1}[n, n]) u_C^k = \tilde{f}_C^k. \quad (3.10)$$

A comparison of the interface equations derived from the purely algebraic decomposition (3.7) with those presented above (3.10) reveals, that the latter no longer depends on the upper right entry of the inverse local matrix $A[1, n]$. This particular entry has been associated with previous complications (see Table 3.2), suggesting that the current method might perform better. Further note, that this scheme is strictly causal on the time slab level, as only the previous time step is involved in the recursion.

3.4.2 Results

Since our goal was to improve on the data presented in Section 3.3.2, we repeat the same experiments for the system arising from continuous domain decomposition. These results are listed in Table 3.3. As expected from the analysis, we no longer observe any difference between an odd or an even number of local degrees of freedom, presenting a big improvement over the purely algebraic decomposition.

Overall, the spectral condition number appears to have marginally improved, compared to the best-case scenario previously observed. However, the influence of the

4 domains	$n_t = 8$	uneven	4 domains	$n_t = 12$	uneven
μ	$\kappa_2(S_C)$	$\kappa_2(P_I^{-1}S_C)$	μ	$\kappa_2(S_C)$	$\kappa_2(P_I^{-1}S_C)$
4	1.69424	1.19897	4	1.69175	1.20075
6	1.38577	1.27207	6	1.38056	1.27688
9	1.17179	1.31933	9	1.1679	1.32371
13.5	1.05078	1.31494	13.5	1.05264	1.31263
20.25	1.0037	1.25804	20.25	1.00865	1.25187
8 domains	$n_t = 16$	uneven	8 domains	$n_t = 24$	uneven
μ	$\kappa_2(S_C)$	$\kappa_2(P_I^{-1}S_C)$	μ	$\kappa_2(S_C)$	$\kappa_2(P_I^{-1}S_C)$
4	3.34312	1.14882	4	3.34774	1.14721
6	2.50469	1.23193	6	2.50452	1.23201
9	1.86639	1.32916	9	1.86071	1.33322
13.5	1.43172	1.41572	13.5	1.42391	1.42348
20.25	1.17026	1.4539	20.25	1.16684	1.45817

Table 3.3: Results of the time casual formulation for different eigenvalues, decompositions and number of local degrees of freedom.

preconditioner is more pronounced, particularly when dealing with a greater number of domains and smaller eigenvalues μ , as illustrated in Table 3.4. In fact, the spectral condition number of the preconditioned system now seems to be independent of the number of subdomains.

domains	$\kappa_2(S_C)$	$\kappa_2(P_I^{-1}S_C)$
4	1.68178	1.20793
8	3.33186	1.15277
16	6.6878	1.08703
32	13.4141	1.04598
64	26.8732	1.02355

Table 3.4: Condition number for different number of time slabs on a fixed small time grid with $n_t = 128$ and Eigenvalue $\mu = 4$.

4 PDE Setting

We now switch our attention to the PDE setting. General results discussing well-posedness and error estimates have already been given in Chapter 2. Our main focus therefore lies in applying the knowledge gained from the ODE setting in the previous chapter. We start by providing a numerical baseline in form of the purely algebraic decomposition, adding on the implicit Euler preconditioner and finally introducing a time causal formulation.

As a model problem, we consider the one-dimensional heat equation with homogeneous initial and boundary conditions on the unit square $Q = \Omega \times (0, 1)$, with $\Omega = (0, 1)$, and with a $C^\infty(Q)$ smooth solution $u(t, x) = \sin(\pi t)\sin(\pi x)$.

$$\begin{aligned} \partial_t u(t, x) - \Delta_x u(t, x) &= f(t, x) & (t, x) &\in (0, 1) \times (0, 1), \\ u(t, x) &= 0 & (t, x) &\in \{0, 1\} \times (0, 1), \\ u(0, x) &= 0 & x &\in (0, 1). \end{aligned} \quad (4.1)$$

We introduce a domain decomposition by splitting the domain $Q = \Omega \times (0, 1)$ into $p > 2$ equally spaced time slices $0 = T_0 < T_1 < \dots < T_p = 1$, where $H = 1/p$, $T_i = iH$ for $i = 0, \dots, p$. Each time slice is therefore given by $Q_i = \Omega \times (T_{i-1}, T_i)$ for $i = 1, \dots, p$.

4.1 Discretization

A uniform tensor product mesh is introduced by splitting the spatial domain into n_x , and the temporal domain into n_t elements respectively. In order to resolve the domain decomposition with this mesh, we need n_t to be a multiple of p . Further, we use piecewise bilinear, globally continuous test and ansatz functions. Refinement is done uniformly by doubling the number of elements in each direction. The local problems from (1.10) are solved using LU decomposition and GMRES [3, Algorithm 9.6] is used as an iterative solver for the global Schur complement system. When considering the ansatz space as a tensor product, i.e. $X_h = W_{h_x} \otimes V_{h_t}$ the linear system of equations $A_h \underline{u} = \underline{f}$ also follows the tensor product structure

$$A_h = M_{h_x} \otimes K_{h_t} + K_{h_x} \otimes M_{h_t}, \quad (4.2)$$

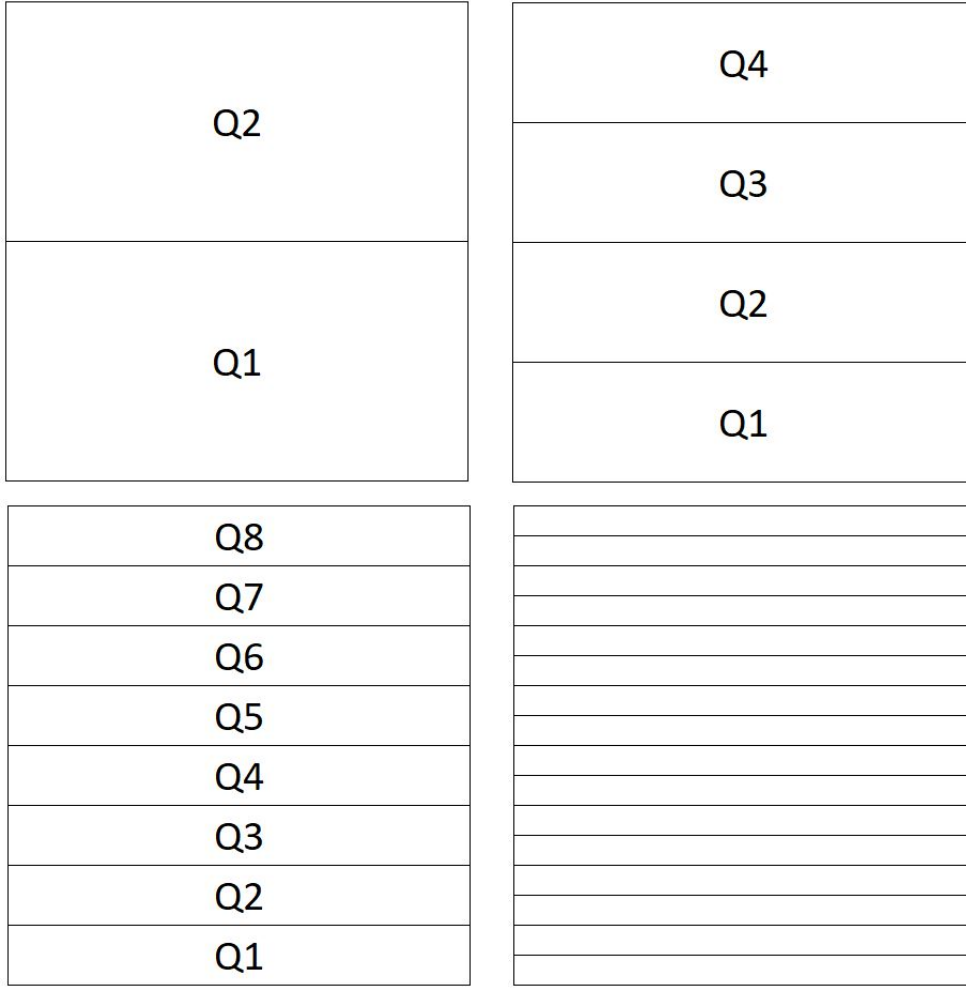


Figure 4.1: The unit square $(0, 1)^2$ split into time slabs for $p = 2, 4, 8, 16$

where

$$\begin{aligned}
 M_{h_x}[j, i] &= \langle \phi_i, \phi_j \rangle_{L^2(\Omega)}, & K_{h_x}[j, i] &= \langle \nabla_x \phi_i, \nabla_x \phi_j \rangle_{L^2(\Omega)}, \\
 M_{h_t}[j, i] &= \langle \phi_i, \phi_j \rangle_{L^2(0,1)}, & K_{h_t}[j, i] &= \langle \partial_t \phi_i, \phi_j \rangle_{L^2(0,1)}.
 \end{aligned}$$

All spatial and temporal matrices are implemented seperatly using MFEM [10]. They are then assembled via the Kronecker tensor product to form the global system of linear equations. Further, linear algebra also uses the Eigen library [5]

4.1.1 Baseline Results

To establish a baseline on what to expect from our method, we start with $n = n_x = n_t = 16$ elements for both the spatial and temporal computational domain. Splitting our domain into $p = 2, 4, 8, 16$ time slices (Figure 4.1) and refining uniformly, gives us a first idea about the behaviour.

$p = 2$				$p = 4$			
dofs[S]	$\ u - u_h\ _{L_2(Q)}$	eoc	iterations	dofs[S]	$\ u - u_h\ _{L_2(Q)}$	eoc	iteration
17	0.00184379	-	1	51	0.00184379	-	3
33	0.000460822	2.00	1	99	0.000460822	2.00	3
65	0.000115198	2.00	1	195	0.000115198	2.00	4
129	2.87989e-05	2.00	1	387	2.87989e-05	2.00	5
257	7.19969e-06	2.00	1	771	7.19969e-06	2.00	7
$p = 8$				$p = 16$			
dofs[S]	$\ u - u_h\ _{L_2(Q)}$	eoc	iterations	dofs[S]	$\ u - u_h\ _{L_2(Q)}$	eoc	iterations
119	0.00184379	-	11	255	0.00184379	-	56
231	0.000460822	2.00	15	495	0.000460822	2.00	45
455	0.000115198	2.00	21	975	0.000115198	2.00	61
903	2.87989e-05	2.00	32	1935	2.87989e-05	2.00	88
1799	7.19969e-06	2.00	45	3855	7.19969e-06	2.00	126

Table 4.1: Baseline results for 2,4,8,16 subdomains

The first observation we can make from Table 4.1 is, that we achieve the expected eoc of 2, ensuring us of a correct implementation.

Further, we observe drastically increasing iteration numbers of the iterative solver, for both more subdomains p and a finer discretization.

As noted in Chapter 1.3, we need to have less than p iterations, in order to have a chance of being more efficient than a sequential solution approach, which is clearly not fulfilled as of now. In fact, this method can be considered to be significantly worse than solving each time slab sequentially, using even a direct solver like LU decomposition. Therefore, we again introduce the implicit Euler preconditioner which showed desirable results already for the ODE setting.

4.2 Implicit Euler Preconditioner

The Schur Complement S can be roughly interpreted as an operator on a coarse grid in time with step $H = 1/p$. One idea to precondition this is to use some time stepping scheme as a coarse grid correction. A straightforward way is to use the implicit Euler method for the semi-discretized PDE.

For the simple ordinary differential equation $\partial_t w(t) = g(t, w)$, the implicit Euler method with step size H and iteration index k reads as

$$w^{k+1} = w^k + Hg(t^{k+1}, w^{k+1}). \quad (4.3)$$

In order to apply this to the heat equation (4.1), we use only integration in space when deriving the variational formulation. This leaves us with a system of ODEs

$$M_h \partial_t \underline{u}(t) + K_h \underline{u}(t) = \underline{f}(t),$$

with $\underline{u}(t) = (u_1(t), u_2(t), \dots, u_{n_x}(t))^T$. M_h and K_h are the standard 1D mass and stiffness matrix with respect to the basis $\{\phi_i\}_{i=1}^{n_x-1}$

$$M_h[i, j] = \int_0^1 \phi_j(x) \phi_i(x) dx,$$

$$K_h[i, j] = \int_0^1 \partial_x \phi_j(x) \partial_x \phi_i(x) dx.$$

This can also easily be seen when replacing the matrices responsible for the temporal discretization with time dependent ansatz functions in the tensor product form of the system matrix (4.2). For a more detailed derivation, see e.g. [3, Section 6.1.4].

Reordering and inserting this into (4.3), we get

$$\begin{aligned} \partial_t \underline{u}(t) &= M_h^{-1}(\underline{f}(t) - K_h \underline{u}(t)), \\ \Rightarrow \underline{u}^{k+1} &= \underline{u}^k + H M_h^{-1}(\underline{f}^{k+1} - K_h \underline{u}^{k+1}), \\ H^{-1}[(M_h + H K_h) \underline{u}^{k+1} - M_h \underline{u}^k] &= \underline{f}^{k+1}. \end{aligned}$$

As already discussed in the ODE setting, the recursion allows a matrix representation, which nicely suits our application

$$P_I \underline{u} = \underline{f},$$

$$P_I = \frac{1}{H} \begin{pmatrix} M_h + H K_h & & & \\ -M_h & \ddots & & \\ & \ddots & \ddots & \\ & & -M_h & M_h + H K_h \end{pmatrix}.$$

Finally, we can apply P_I as a left preconditioner yielding the system to solve

$$\begin{aligned} S u_C &= f, \\ P_I^{-1} S u_C &= P_I^{-1} f. \end{aligned}$$

p = 2				p = 4			
dofs [S]	$\ u - u_h\ _{L_2(Q)}$	eoc	iterations	dofs [S]	$\ u - u_h\ _{L_2(Q)}$	eoc	iterations
17	0.00184379	-	1	51	0.00184379	-	3
33	0.000460822	2.00	1	99	0.000460822	2.00	3
65	0.000115198	2.00	1	195	0.000115198	2.00	3
129	2.87989e-05	2.00	1	387	2.87989e-05	2.00	3
257	7.19969e-06	2.00	1	771	7.19969e-06	2.00	3

p = 8				p = 16			
dofs [S]	$\ u - u_h\ _{L_2(Q)}$	eoc	iterations	dofs [S]	$\ u - u_h\ _{L_2(Q)}$	eoc	iterations
119	0.00184379	-	7	255	0.00184379	-	15
231	0.000460822	2.00	7	495	0.000460822	2.00039	15
455	0.000115198	2.00	7	975	0.000115198	2.0001	15
903	2.87989e-05	2.00	7	1935	2.87989e-05	2.00003	15
1799	7.19969e-06	2.00	7	3855	7.19969e-06	2.00001	15

Table 4.2: Results with implicit Euler Preconditioner for 2,4,8,16 subdomains

4.3 Results after Preconditioning

Again, Table 4.2 confirms the eoc of 2 as we would expect, and also the error values are comparable with those from Table 4.1.

When looking at iteration numbers, we can observe unchanging values with respect to refinement. This hints, that we have successfully eliminated a dependency on the local mesh size h . Also, Table 4.3 shows a significant decrease in the spectral condition number κ_2 , when the preconditioner is applied to the Schur complement S . This also implies a good effect of the preconditioner.

On the other hand, the iterations seem to increase linearly with the number of subdomains, giving values oddly reminiscent of simply solving the local problems sequentially. In fact, when considering perfect speed-up and no overhead, this method would only be able to match a sequential approach and does not gain any advantage.

Although this can be considered a first success, there are still more improvements needed for this method to be viable.

Influence of the Number of Local Degrees of Freedom

Already in the ODE setting, we observed an impact of the number of local degrees of freedom on the conditioning of the Schur complement. It can be expected to see a similar behaviour, also in the full PDE setting. We try to replicate the ODE setting by using only $n_x = 2$ elements in the spatial direction. This can be seen as having 1 degree of freedom representing only the largest eigenvalue of the spatial Laplacian. Refining once only in the spatial direction gives us an insight into the combined be-

p = 2			p = 4		
dofs [S]	$\kappa_2(S)$	$\kappa_2(PS)$	dofs [S]	$\kappa_2(S)$	$\kappa_2(PS)$
17	104.889	18.8793	51	326.942	55.457
33	371.297	41.8532	99	1143.58	121.058
65	1294.64	99.7697	195	3953.93	283.994
129	4460.47	253.058	387	13546	710.192
257	15247.4	672.058	771	46129.5	1866.73

p = 8			p = 16		
dofs [S]	$\kappa_2(S)$	$\kappa_2(PS)$	dofs [S]	$\kappa_2(S)$	$\kappa_2(PS)$
119	873.346	131.905	255	2991.76	363.212
231	2921.06	283.464	495	7666.96	641.377
455	9837.24	664.083	975	24403.3	1501.85
903	33066.1	1660.41	1935	79064.3	3799.51
1799	111103	4364.73	3855	258049	10080.5

Table 4.3: Spectral condition number with and without preconditioner for 2,4,8,16 subdomains

haviour with larger eigenvalues.

Judging on the data given in Table 4.4, the effect of odd/even differences present in the ODE do not seem to fully carry over and are less pronounced. But especially for 8 time slabs, the negative impact of the preconditioner is still quite obvious. Larger eigenvalues seem to even out the effect in our favour, given that a finer spatial grid introduces larger eigenvalues.

4 time slabs	nt = 8	uneven	4 time slabs	nt = 12	even
n_x	$\kappa_2(S_C)$	$\kappa_2(P_I^{-1}S_C)$	n_x	$\kappa_2(S_C)$	$\kappa_2(P_I^{-1}S_C)$
2	3.44975	3.11033	2	3.2455	3.74573
4	15.5012	9.46021	4	12.7601	10.9386

8 time slabs	nt = 16	uneven	8 time slabs	nt = 24	even
n_x	$\kappa_2(S_C)$	$\kappa_2(P_I^{-1}S_C)$	n_x	$\kappa_2(S_C)$	$\kappa_2(P_I^{-1}S_C)$
2	12.452	8.50762	2	8.25461	11.5925
4	32.2428	28.3518	4	25.2261	31.7593

Table 4.4: Spectral condition number κ_2 with and without the preconditioner applied.

4.4 Time Causal Space-Time FEM for the Heat Equation

Already in the ODE setting, a combination of the purely algebraic domain decomposition and a decomposed time causal formulation proved to be the most successful, especially in eliminating the dependency on odd/even case.

Let $0 = T_0 < T_1 < \dots < T_p = 1$ be a decomposition of the interval $(0, 1)$ into p time slices. We reformulate the heat equation (2.1) on each time slice as

$$\partial_t u^m(x, t) + \Delta_x u^m(x, t) = f(x, t) \quad (x, t) \in Q_m = (0, 1) \times (T_{m-1}, T_m), \quad (4.4)$$

$$u_m(T_{m-1}) = u_{m-1}(T_{m-1}), \quad (4.5)$$

for $m = 1, \dots, p$, with $u_0(T_0) = 0$.

4.4.1 Discretization and Matrix Assembly

We now use a uniform tensor product mesh on each time slice Q_m , with piecewise linear test and ansatz functions. This yields the standard variational formulation, restricted to each time slice Q_m , to find $u_h^m \in S_h^1(Q_m)$ such that

$$\int_{Q_m} [\partial_t u_h^m v_h + \nabla_x u_h^m \cdot \nabla_x v_h] dx dt = \int_{Q_m} f v_h dx dt \quad \forall v_h \in S_h^1(Q_m).$$

From this we get the local system matrices A_m for the unhomogenized systems

$$A_m \underline{u}^m = \underline{f}^m.$$

We can use a splitting approach to homogenize the initial condition

$$\underline{u}^m = \underline{u}_I^m + \underline{u}_H^m = (\underline{u}^{m-1}[end], 0, \dots, 0)^\top + (0, \underline{u}^m[2 : end]^\top)^\top.$$

This leaves us with the linear system of equations for each time slice

$$\begin{aligned} A_m(\underline{u}_I^m + \underline{u}_H^m) &= \underline{f}^m, \\ A_m[:, 1] \underline{u}^{m-1}[end] + A_m[:, 2 : end] \underline{u}_H^m &= \underline{f}^m. \end{aligned}$$

Finally, we can assemble the global system matrix by overlapping the columns at each interface node

$$\begin{pmatrix} A_1[:, 1 : end - 1] & A_1[:, end] & & & \\ & A_2[:, 1] & A_2[:, 2 : end - 1] & A_2[:, end] & \\ & & \ddots & & \\ & & & A_m[:, 1] & A_m[:, 2 : end] \end{pmatrix}.$$

4.4.2 Results

Previously, we have only compared iteration numbers for the PDE setting. Even though this is what we are finally interested in, looking at the spectral condition number might be the more precise approach.

Therefore, we rerun the experiments for the purely algebraic decomposition in Section 4.1.1, now including the spectral condition number. This can be seen in Table 4.5, for both an even and uneven number of local dofs. Table 4.6 shows the results for the new time causal formulation. In Figure 4.2 we compare the data from both Tables in a graphical way. There, we can see a visible improvement of the spectral condition number of the system matrix S , when using the time causal approach. When applying the preconditioner on the other hand, the purely algebraic decomposition is better conditioned. Especially for larger p , the difference in conditioning between both preconditioned systems decreases. This hints, that for even more subdomains, we might actually see improvements.

4 domains	$n = 8$	uneven	4 domains	$n = 12$	even
$dofs$	$\kappa_2(S)$	$\kappa_2(P_I^{-1}S)$	$dofs$	$\kappa_2(S)$	$\kappa_2(P_I^{-1}S)$
21	87.3825	21.7107	33	191.538	35.6738
45	320.252	49.4155	69	672.968	80.7508
93	1134.29	115.057	141	2353.96	191.678
8 domains	$n = 16$	uneven	8 domains	$n = 24$	even
$dofs$	$\kappa_2(S)$	$\kappa_2(P_I^{-1}S)$	$dofs$	$\kappa_2(S)$	$\kappa_2(P_I^{-1}S)$
105	856.882	117.792	161	1816.81	179.058
217	2897.79	269.462	329	5915.52	448.389
441	9801.13	649.938	665	19946.4	1112.64

Table 4.5: Spectral condition number for the purely algebraic decomposition with implicit euler preconditioner for both odd and even cases.

Since the formulations are slightly different, we compare the error values in Table 4.7. This shows, that as expected, the sequential formulation loses some accuracy compared to the purely algebraic approach. An increasing number of subdomains amplifies this effect. We suspect that each interface introduces an error.

Table 4.7 also shows the iteration numbers for both formulations, where we can see no difference.

More domains

Until now, we were not able to see any improvement as we would have expected from the analysis done in the ODE setting. One could suspect that differences only show

4 domains	$n = 8$	uneven	4 domains	$n = 12$	even
$dofs$	$\kappa_2(S)$	$\kappa_2(P_I^{-1}S)$	$dofs$	$\kappa_2(S)$	$\kappa_2(P_I^{-1}S)$
21	51.755	24.7197	33	112.932	41.294
45	182.678	63.1483	69	381.311	110.126
93	640.673	164.42	141	1326.12	291.984
8 domains	$n = 16$	uneven	8 domains	$n = 24$	even
$dofs$	$\kappa_2(S)$	$\kappa_2(P_I^{-1}S)$	$dofs$	$\kappa_2(S)$	$\kappa_2(P_I^{-1}S)$
105	406.891	142.294	161	996.49	204.906
217	1433.39	364.355	329	2992.98	642.717
441	5029.13	968.216	665	10410.4	1739.62

Table 4.6: Spectral condition number for the time causal formulation with implicit euler preconditioner for both even and uneven case

p	dofs[S]	$\ u - u_h\ _{L_2(Q)}$	$\ \tilde{u} - \tilde{u}_h\ _{L_2(Q)}$	iter	iter sequ
2	15	0.00184379	0.002207	1	1
	31	0.000460822	0.000550492	1	1
	63	0.000115198	0.000137539	1	1
4	45	0.00184379	0.00233153	3	3
	93	0.000460822	0.000581831	3	3
	189	0.000115198	0.000145387	3	3
8	105	0.00184379	0.00240461	7	7
	217	0.000460822	0.000600417	7	7
	441	0.000115198	0.000150053	7	7

Table 4.7: Comparison of the two methods with u_h the solution of the purely algebraic decomposition and \tilde{u}_h the solution for the time causal formulation, both with the preconditioner P_I applied. $n_t = n_x = 16$ and refining uniformly.

up when using a higher number of subdomains. Therefore, we extend our experiments to investigate this.

Although Table 4.8 shows that the spectral condition number of the time causal formulation is worse after applying the preconditioner compared to the purely algebraic decomposition with the same preconditioner, we see iteration numbers stagnate and actually decrease for more than 8 domains. Figure 4.3 nicely highlights the linear increase in iteration numbers for the algebraic formulation compared to the almost constant one for the time causal formulation.

Finally, this means that we have achieved a feasible strategy, gaining an advantage over simply solving the local problems sequentially.

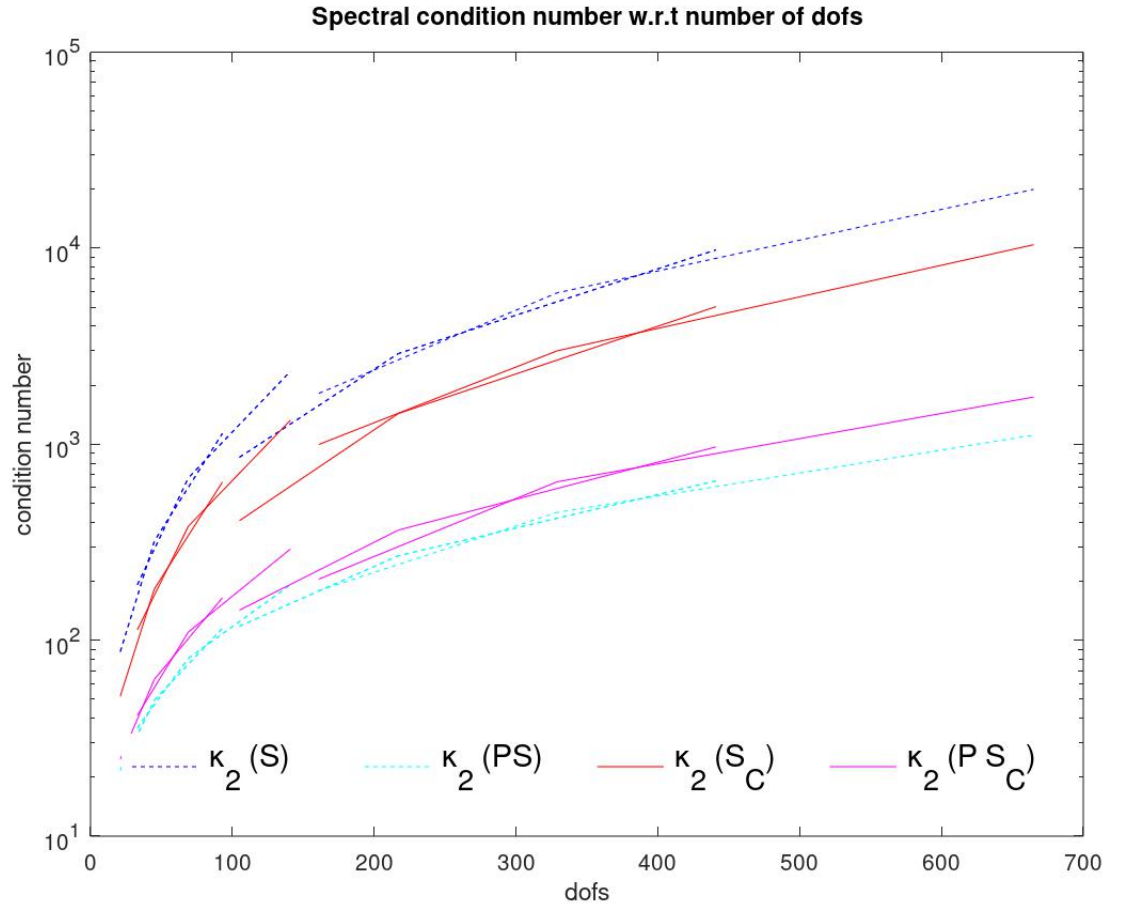


Figure 4.2: Comparison of the spectral condition numbers for both formulations representing Table 4.5 and Table 4.6. The purely algebraic system matrix is denoted by S and dotted lines in the plot. S_C denotes the system matrix for the time causal formulation. Corresponding results are represented as solid lines. P denotes the inverse implicit euler matrix used as preconditioner.

time causal				standard			
domains	$\kappa_2(S)$	$\kappa_2(PS)$	iterations	domains	$\kappa_2(S)$	$\kappa_2(PS)$	iterations
2	2548.06	443.333	1	2	4452.54	250.871	1
4	7603.63	1216.55	3	4	13521.9	703.796	3
8	17404.9	2649.31	7	8	33007.4	1645.49	7
16	36225.1	5569.49	7	16	78924.4	3766.76	15
32	71719.3	11670.7	6	32	197888	8382.99	31
64	139037	24278.7	5				

Table 4.8: Spectral condition number and iteration number comparing the different formulations on a fixed 128×128 grid with different number of subdomains.

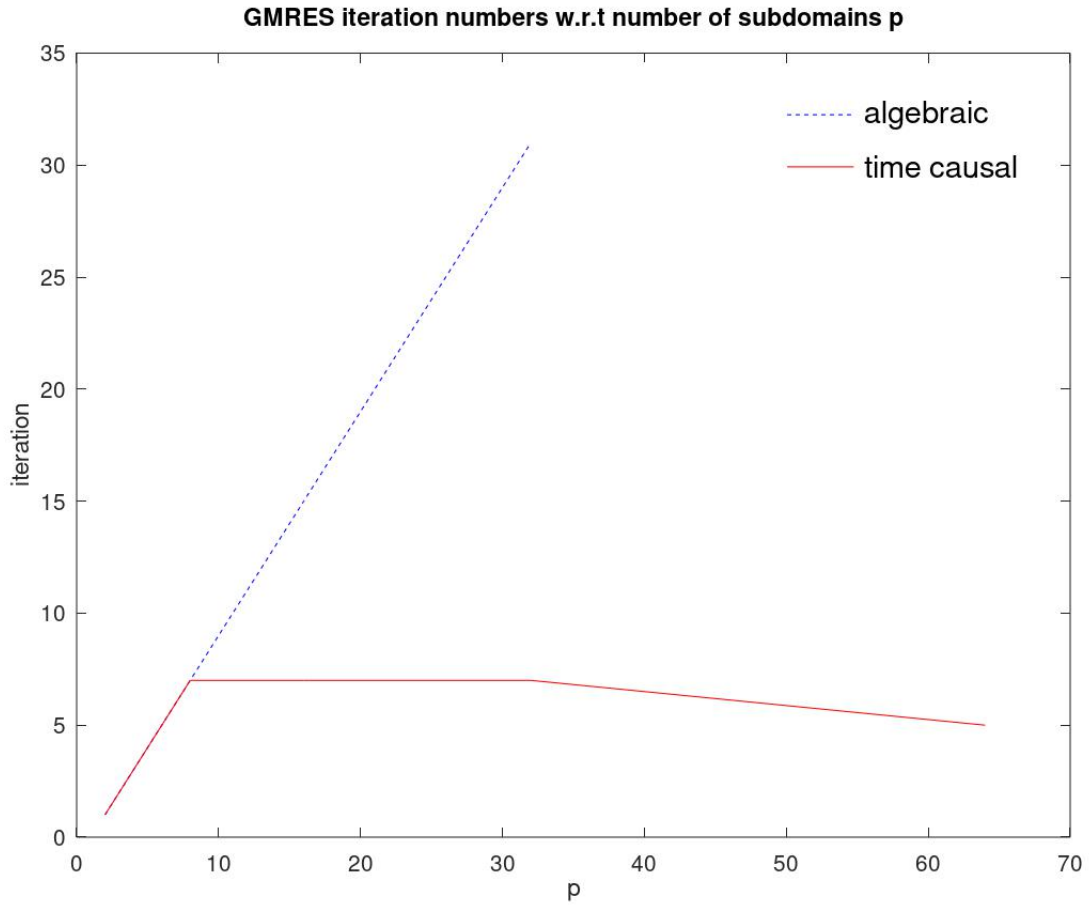


Figure 4.3: Table 4.8 represented graphically.

5 Conclusion

This work has successfully explored domain decomposition methods for the finite element discretization of the heat equation comparable to the Parareal algorithm [9]. We have found that an efficient way to analyse the Schur complement is achieved using the ODE setting. We were able to reproduce problems identified in the ODE setting also for the PDE. Therefore, also the solution approach was applicable, which left us with desirable results. Also the results coming from the analysis on the Schur complement in the ODE setting shed light on how the eigenvalue μ affects the overall conditioning. Although first numerical experiments look very promising, the data is still quite limited. One should consider less smooth model problems in order to see a more distinctive separation between the simulations. Further, one could replace the implicit Euler scheme with any higher order scheme and observe the effect. Since no real parallel implementation was done, all considerations concerning speedup are purely theoretical and may not represent the real world application. A different approach to preconditioning was done in [4] using boundary integral equations, which works for more general domain decomposition but involves more computational effort in setting up the preconditioner. This also showed constant iterations but no comparable decompositions have been considered.

Bibliography

- [1] W. Arendt and K. Urban. *Partielle Differenzialgleichungen: Eine Einführung in analytische und numerische Methoden*. Springer Berlin Heidelberg, 2018.
- [2] J. W. Eaton, D. Bateman, S. Hauberg, and R. Wehbring. *GNU Octave version 5.2.0 manual: a high-level interactive language for numerical computations*, 2020.
- [3] A. Ern and J.-L. Guermond. *Theory and practice of finite elements*, volume 159 of *Applied Mathematical Sciences*. Springer-Verlag, New York, 2004.
- [4] P. Gaulhofer. A preconditioned schur complement solver for the space-time discretization of the one-dimensional heat equation. Bakkalaureatsprojekt TM, Institut für Numerische Mathematik, Technische Universität Graz, 2022.
- [5] G. Guennebaud, B. Jacob, et al. Eigen v3. <http://eigen.tuxfamily.org>, 2010.
- [6] M. Kreuter. Sobolev spaces of vector-valued functions. Master’s thesis, Ulm University, Faculty of Mathematics and Economics, 2015.
- [7] C. Köthe, R. Löscher, and O. Steinbach. Adaptive least-squares space-time finite element methods. arXiv:2309.14300, 2023.
- [8] U. Langer, O. Steinbach, and H. Yang. Robust space-time finite element methods for parabolic distributed optimal control problems with energy regularization. *Adv. Comput. Math.*, 50(2):Paper No. 24, 30, 2024.
- [9] J.-L. Lions, Y. Maday, and G. Turinici. Résolution d’EDP par un schéma en temps “pararéel”. *C. R. Acad. Sci. Paris Sér. I Math.*, 332(7):661–668, 2001.
- [10] MFEM: Modular finite element methods [Software]. mfem.org.
- [11] O. Steinbach. Space-time finite element methods for parabolic problems. *Comput. Methods in Appl. Math.*, 15(4):551–566, 2015.
- [12] O. Steinbach and P. Gaulhofer. On space-time finite element domain decomposition methods for the heat equation. In *Domain decomposition methods in science and engineering XXVI*, volume 145 of *Lect. Notes Comput. Sci. Eng.*, pages 547–554. Springer, Cham, [2022] ©2022.
- [13] O. Steinbach and H. Yang. Space-time finite element methods for parabolic evolution equations: discretization, a posteriori error estimation, adaptivity and solution. In *Space-time methods—applications to partial differential equations*, volume 25 of *Radon Ser. Comput. Appl. Math.*, pages 207–248. De Gruyter, Berlin, [2019] ©2019.

- [14] O. Steinbach and M. Zank. Coercive space-time finite element methods for initial boundary value problems. *Electron. Trans. Numer. Anal.*, 52:154–194, 2020.
- [15] M. Zank. *Inf-sup stable space-time methods for time-dependent partial differential equations*. PhD thesis, Technischen Universität Graz, 2020.